CONF-951073--21
BNL-62554
To be published in the Conference Record of the 1995 IEEE Nuclear Science Symposium/Medical Imaging Conference, October 21-28, 1995, San Francisco, CA (revised 12/01/95)



# Dual Energy Iodine Contrast CT with Monochromatic X Rays

F.A. Dilmanian, X.Y. Wu, J. Kress, B. Ren, D. Chapman, J.A. Coderre, D. Greenberg, E. Parsons, M. Shleifer, D.N. Slatkin, W.C. Thomlinson, and Z. Zhong, Brookhaven National Laboratory; T.M. Button, F. Giron, J. Liang, M.J. Petersen, and C.T. Roque, State University of New York at Stony Brook; M.H. Miller, and H. Weedon, Analogic Corp.; D.J. Krus, and L. Perna, Bicron; and K. Yamamoto, Hamamatsu

*Abstract*

Computed tomography (CT) with monochromatic x-ray beams was used to image phantoms and a live rabbit using the preclinical Multiple Energy Computed Tomography (MECT) system at the National Synchrotron Light Source. MECT has a horizontal fan beam with a subject apparatus rotating about a vertical axis. Images were obtained at 43 keV for single-energy studies, and at energies immediately below and above the 33.17 keV iodine K-edge for dual-energy subtraction CT. Two $CdWO_4$-photodiode array detectors were used. The high-resolution detector (0.5 mm pitch, uncollimated) provided 14 line pair/cm in-plane spatial resolution, with lower image noise than conventional CT. Images with the low-resolution detector (1.844-mm pitch, collimated to 0.922 mm detector elements) had a sensitivity for iodine of ≈ 60 μg/cc in 11-mm channels inside a 135 mm-diameter acrylic cylindrical phantom for a slice height of 2.5 mm and a surface dose of ≈ 4 cGy. The image noise was ≈ 1 Hounsfield Unit (HU); it was ≈ 3 HU for the same phantom imaged with conventional CT at approximately the same dose, slice height, and spatial resolution (≈ 7 lp/cm). These results show the potential advantage of MECT, despite present technical limitations.

## I. INTRODUCTION

Substantial advances have been made in techniques of computed tomography since its invention in the 1960s and 70s. They include improvements in the source, detector, gantry, data acquisition system and system control, image processing, corrections and display, and in the development of clinical applications. Milestones include the development of high-resolution CT, including dynamic focal spot, as well as dual-slice scanning [1], Helical (or Spiral) [2], and the Ultrafast [3] CT. Nevertheless, the problem of the large beam-energy width is unresolved because these systems employ bremsstrahlung radiation which inherently has a broad energy spectrum. Development of high-intensity synchrotron x-ray beamlines in the last decade paved the way to the evolution of the first monochromatic CT systems [4-8] which should answer the basic question on the image quality improvements one should expect from the use of monochromatic beams.

This paper characterizes such a system, multiple energy computed tomography (MECT), which is under development at the X17B superconducting wiggler beam line of the National Synchrotron Light Source, Brookhaven National Laboratory (BNL) [5-7], and presents single- and dual-energy results from the preclinical MECT. The rationale for the development of MECT has been to establish the performance of monochromatic CT, and to apply the system to clinical research in neuroradiology, atherosclerosis imaging, and CT angiography.

Research supported by the Office of Health and Environmental Research of U.S. Department of Energy.

## II. ADVANTAGES OF MONOCHROMATIC CT

1. Beam-hardening artifacts [9] are eliminated in monochromatic CT, so improving the contrast resolution and the quantification accuracy of the images. The improvements depend on tissue non-uniformities in the subject.

2. Monochromatic CT at optimized beam energy for a patient's size minimizes the absorbed dose to the patient by eliminating the lower end of the polychromatic energy spectrum. It also improves image contrast by eliminating the higher end of the polychromatic energy spectrum which is associated with low image contrast.

3. In contrast imaging, a substantial gain (i.e. ≈ 2 fold or more) is achieved when the monochromatic beam energy is tuned just above the K-edge of the contrast element [10] (for iodine, K-edge of 33.17 keV, the K-edge rise in the attenuation is ≈ 5.6 fold). Furthermore, the contrast agent is better quantified by subtracting the below-edge image from the above-edge image. Because the beam energy in this method is lower than the mean beam energy in contrast imaging with conventional CT, its possible clinical use may encourage development of heavier CT contrast elements (e.g., Gadolinium, K-edge = 50.23 keV).

4. Monochromatic CT is much more suitable for Dual-Energy Quantitative CT (DEQCT, Ref. 11) than is polychromatic CT. This powerful method, generally called dual photon absorptiometry (DPA), allows definition of the tissue into a low-Z and an intermediate-Z element group in terms of separate CT images.

The first three effects were quantified by Monte Carlo Simulations [12].

Clinical research with MECT is expected to include DPA imaging for quantification of carotid artery atherosclerotic plaque evolution, i.e., delineation of fatty, fibrous, and necrotic (non-calcified and calcified) tissues, and KES of iodine or gadolinium for CT angiography.

## III. MECT SYSTEM DESIGN

### A. Monochromator

The monochromator is a tunable, two-crystal Laue-Laue device, producing a monochromatic beam parallel to the incident white beam, with a vertical offset of 15 mm independent of beam energy [13]. It uses flat Si <111> crystals mounted on independent joystick (gimbal) mechanisms, and has a 24.5 - 51.2 keV energy range.

### B. Detectors

Two different modular $CdWO_4$-photodiode linear array detectors were used, both employing PIN (p-type intrinsic n-type) diodes. The first (referred to as the high-resolution) was used for imaging the rabbit and the ring phantom presented below; however, it later exhibited excessive differential non-linearity. The second one was on loan from Analogic Corp. [14]. Their specifications are as follows:

| | High resolution | Low resolution |
|---|---|---|
| Center-to-center element spacing | 0.5 mm | 1.844 mm |
| Element height | 6.0 mm | 28.0 mm |
| Scintillator thickness | 3.5 mm | 2.4 mm |
| Number of elements in a module | 32 | 16 |
| Detector collimation | None | 0.922 mm |

### C. Data acquisition system

The front-end data acquisition system (DAS) with a signal dynamic range of $10^6$:1 was developed by Analogic Corp. [14]. It is connected to an Alpha Computer (Digital Corp.) through a custom-designed interface board fabricated at BNL via a direct-memory access (DMA) board that sits on Alpha's turbochannel bus. From the computer's memory, the data flow to a high-speed disk, using a pair of buffer memories at each step to allow uninterrupted data collection. The interface allows a sustained data flow rate of 1.4 Mbyte/s, its duration limited only by the 1 Gbyte disk.

### D. Image reconstruction Program

The image reconstruction program, developed by the MECT group [15], uses the filtered backprojection method; filtration is carried out in the Fourier space and the backprojection is executed in the configuration space. The program does not have a fixed center point for the backprojection process, e.g. detector center; the center point is a free parameter adjusted by the user.

## IV. EXPERIMENTS AND RESULTS

### A. Method of data collection

Images were acquired with the following parameters: viewing rate of 1440 Hz, rotation speed of 24° $s^{-1}$, and slice thickness of 2.0 mm for the high-resolution images and 2.5 mm for the others. Fig. 1 shows the vertical profile of the monochromatic beam. The monochromator was detuned to 10-20 % peak intensity, keeping the dose-rate to a constant value for single beam energy. Two separate 360°-image data were collected with a 1/2 element-spacing lateral translation of the subject's rotation axis between them. These two images were interlaced during the reconstruction [6, 16]. Reference data, i.e. with no subject in the beam ("air" data) used to calculate the absolute transmission were collected before and after each slice; this minimized variations in the beam profile's shape due to instabilities in the monochromator. Nevertheless, their uncorrected effect, which amounted to ≈ 0.2% for the typical 60 s time elapse between two consecutive air measurements, is the main limit to the image quality of the system. Detector dark-current was measured once every few hours. Temporal variations (i.e. random oscillations) in the beam's intensity were accounted for by using the two unattenuated extremes of the fan beam (called "air channels"). Linear variations of the beam profile's shape were corrected by linear interpolation between these two beam ends [16].

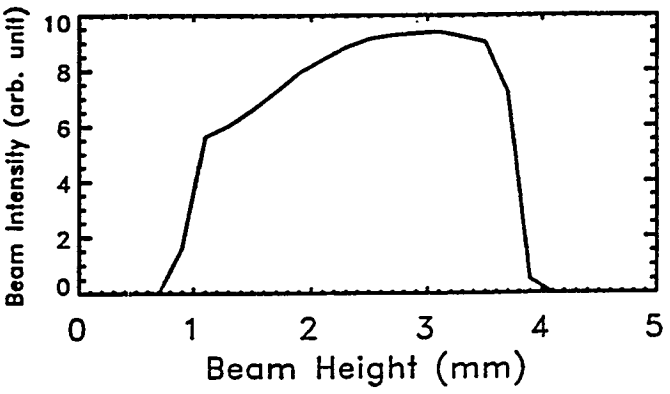


Fig. 1. The vertical profile of the monochromatic beam.

### B. Results

*1. Rabbit neck*: An anesthetized rabbit was imaged at 43 keV at the level of the brain stem (Fig. 2), using the high-resolution detector. The image, with an average diameter of ≈ 13 cm, clearly delineates muscle and subcutaneous fat. It was reconstructed with a Hanning filter with a cutoff at 60% of the Nyquist frequency. The skin absorbed dose was ≈ 4 cGy. A similar slice was imaged with a conventional CT at 80 kVp and 200 mAs (Fig. 3); the dose was 0.7 Gy which, for the 3-mm slice (vs. 2 mm for MECT) is equivalent to 1.0 cGy. The two dark bands along the continuation of the jaw line in the polychromatic image may be beam-hardening effects.

## DISCLAIMER

Fig. 2. MECT image of a rabbit neck at 43 keV and 4 cGy.

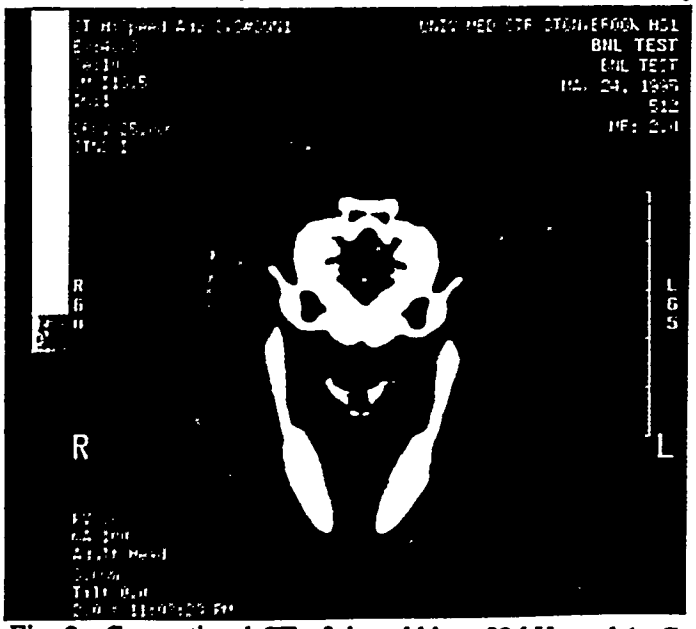


Fig. 3. Conventional CT of the rabbit at 80 kVp and 1 cGy.

2. *Ring phantom*: The phantom was an acrylic cylinder of 98 mm diameter, with concentric 4 mm-deep air grooves in its upper surface. The grooves had equal wall and valley thicknesses that decreased with increasing radius, and reached 0.3 mm at the cylinder's edge (Fig. 4). The phantom was imaged with the high-resolution detector at 43 keV and at ≈ 4 cGy surface dose. The reconstruction used a ramp filter with the Nyquist cutoff frequency. The clover-leaf background pattern is an artifact of digital photography. The last groove is visible.

3. *Iodine phantom*: This phantom, imaged with the low-resolution detector, was a 135-mm diameter acrylic cylinder containing thirty 11-mm diameter paraxial cylindrical channels. The pattern of the channels (Fig. 5) included 5

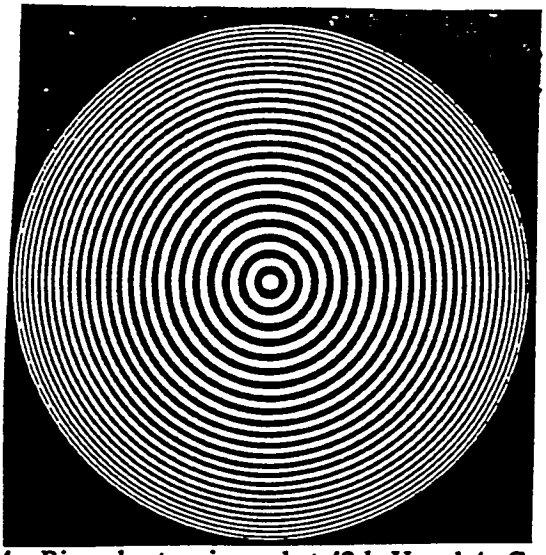

Fig. 4. Ring phantom imaged at 43 keV and 4 cGy dose.

arrays of 6 channels each, positioned along 36°-apart diameters of the cylinder's base (Fig. 5). In each set, five channels were filled with iodine solutions of 240, 120, 60, 30, and 15 I $\mu$g/cc, and one with distilled water. The phantom was imaged with MECT (at 43 keV and 2.3 mm slice, Fig. 6) and with conventional CT (at 80 kVp and 3 mm slice, not shown). The dose was 3.4 cGy with MECT, and 800 mAs (2.8 cGy, equivalent to 3.7 cGy for the same slice heights) with conventional CT. The images were reconstructed with similar filters and filter cut-off frequencies of 0.5 Nyquist frequency. The plot of the CT numbers in the second circle of channels in the MECT and the conventional CT images are shown in Fig. 7 top and bottom, respectively. The image noise was ≈ 1 HU for MECT and ≈ 3 HU for the conventional CT. The spatial resolution was ≈ 7 lp/cm for both.

Figs. 8 show the same phantom imaged with MECT (from left to right) above the edge (33.25 keV), below the edge (33.09 keV) of iodine, and subtracted (i.e. "above" - "below"), respectively. The surface dose was ≈ 4.4 cGy at each energy. The subtracted image was calculated using:

$$\rho_I = 0.0342 \times (1.00564\ \mu_2 - \mu_1)$$

where $\rho_I$ is I concentration in g/cm$^3$, and $\mu_1$ and $\mu_2$ are the I linear attenuation coefficients in units of cm$^{-1}$ at 33.09 and 33.25 keV, respectively.

The results indicate the advantages of MECT images over conventional CT. Furthermore, in the MECT images most of the 60 $\mu$g I/cc channels are visible for both the 43-keV and for the above-the-edge image.

4. *Low-contrast standard phantom*: The phantom was a 105-mm diameter acrylic cylinder that includes two conical inserts of the Gammex RMI [17] standard CT phantom inserts. These were the low contrast insert (part No. 460-013A) with 5 cylindrical inserts of 8.0, 5.6, 4.0, 2.8, and 2.0 mm diameter of 0.6% contrast, and the plain insert (part No. 460-010). Figs. 9 and 10 show MECT and the conventional CT images of the phantom with the low-contrast insert on the left. The images were taken for similar beam energies (43 keV for

MECT, 100 kVp for conventional CT), and had comparable spatial resolutions. The surface dose was 4.4 cGy for MECT and equivalent to 3.1 cGy for conventional CT. All five inserts detectable in the MECT image; only 4 are in the Conventional CT image. The image noise (S.D.) was ≈ 1.5 HU for MECT and ≈ 3 HU for conventional CT.

## V. SUMMARY AND CONCLUSIONS

Despite the technical limitations of the present MECT system, including the beam profile instability, and the large detector pitch that required detector collimation, MECT images show advantage over those of the conventional CT. A bent Laue-Laue monochromator [18] using Si<331> crystals is being developed to alleviate the problem of beam-profile instability. Development of a new detector with 0.8-mm element pitch is also underway.

The clinical MECT system will be completed with development of both the monochromator sections, a patient chair, the new detector, and the patient's safety system. Although the applicability of MECT to clinical research in atherosclerotic plaque imaging is quite certain, its potential in earlier detection of neurological disorders can be studied only with patients.

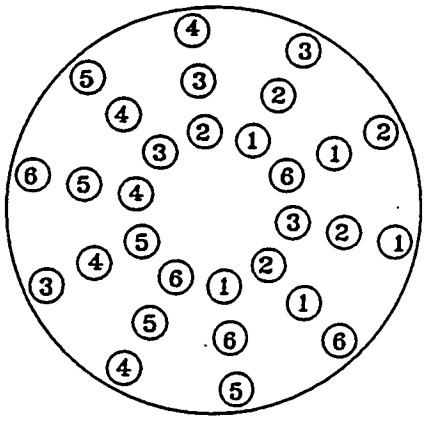

Iodine Concentration:

1: 240 μg I/cc
2: 120 μg I/cc
3: 60 μg I/cc
4: 30 μg I/cc
5: 15 μg I/cc
6: 0 μg I/cc

Fig. 5. Pattern of the iodine solutions in the phantom.

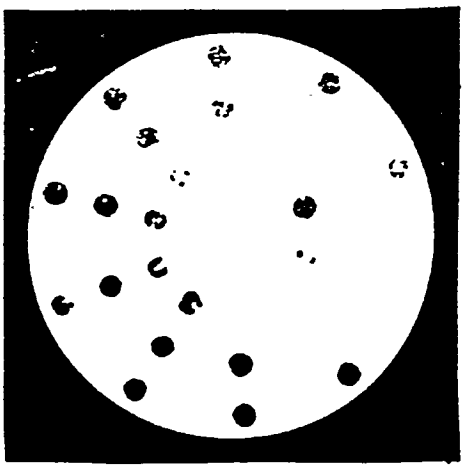

Fig. 6. MECT image of the iodine phantom at 43 keV.

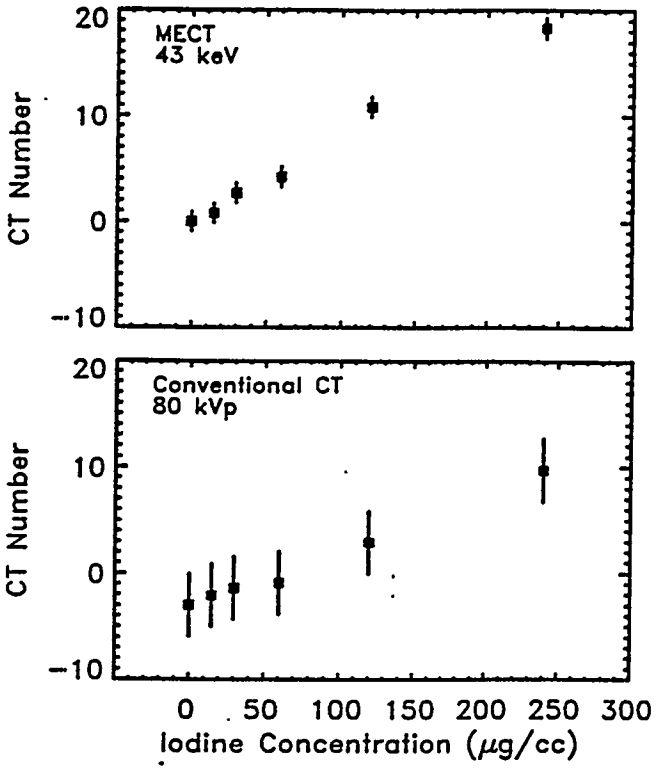


Fig. 7. CT #s in iodine channels: MECT vs. conventional CT.

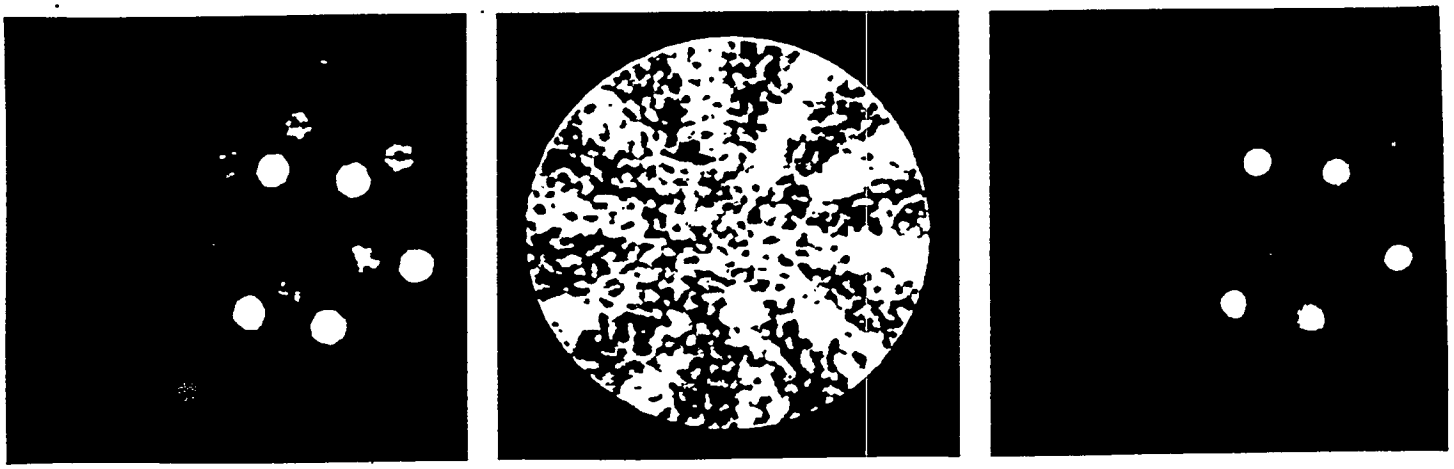

Fig. 8. I phantom: above K-edge, below, and subtraction.

In particular, DPA imaging of the arterial wall will be used to delineate the atherosclerotic plaque composition into fatty, fibrous, and necrotic (non-calcified and calcified) tissues.

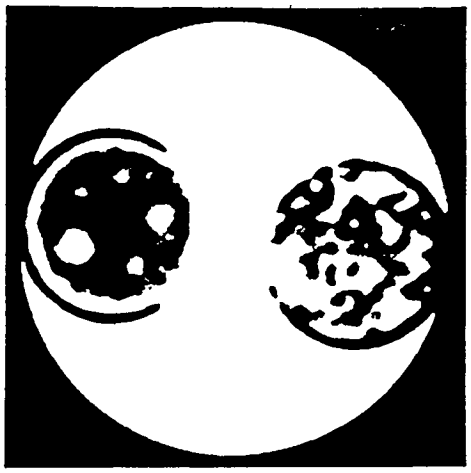

Fig. 9. MECT image of a phantom with a low-contrast insert.

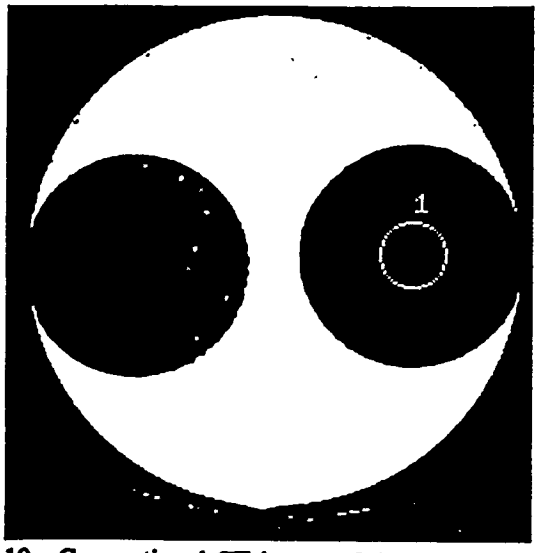


Fig. 10. Conventional CT image of the phantom of Fig. 9.

## ACKNOWLEDGEMENTS

We thank our following colleagues for their help with this research: E.F. Becker and S. Marcovici (Analogic Corp.); L.E. Berman, J.F. Gatz, N.F. Gmür, J.B. Hastings, X. Huang, D.D. Joel, M. Kershaw, A. Lenhard, E. McKenna, R. Menk, P.L. Micca, M.M. Nawrocky, M. Radulescu, D.P. Siddons, G.C. Smith, F.A. Staicu, G.M. Van derlaske, and M.H. Woodle (BNL); J. Arenson and E. Dafni (Elscint, Ltd., Haifa, Israel); and G. Gindi and P. Stephens (SUNY at Stony Brook). We also thank A.D. Woodhead for comments on the manuscript, and A.L. Ruggiero for technical assistance.

## REFERENCES

[1] J. Arenson, Data collection strategies: gantries and detectors. In: "Medical CT and Ultrasound: Current Technology and Applications", L.W. Goldman and J.B. Fowlkers, Eds., American Assoc. of Physicists in Med. College Park, NY, 1995., pp. 329-348.

[2] W.A. Kalender, Principles and performance of Spiral CT. *ibid*, pp. 379-410.

[3] C.H. McCollough, Principles and performance of Electron Beam CT. *ibid*, pp. 411-436.

[4] A.C. Thompson, J. Llacer, L. Campbell Finman, E.B. Hughes, J.N. Otis, S. Wilson, and H.D. Zeman, Computed tomography using synchrotron radiation. Nucl. Instr. and Meth. *222*, 319-323, 1984.

[5] F.A. Dilmanian, R.F. Garrett, W.C. Thomlinson, L.E. Berman, L.D. Chapman, J.B. Hastings, P.N. Luke, T. Oversluizen, D.P. Siddons, D.N. Slatkin, V. Stojanoff, A.C. Thompson, N.D. Volkow, and H.D. Zeman, Computed tomography with monochromatic x rays from the National Synchrotron Light Source, Nucl. Instrum. Methods *B 56/57*, 1208-1213, 1991.

[6] F.A. Dilmanian, Computed tomography with monochromatic x rays, Am. J. Physiol. Imag. *3/4*, 175-193, 1992.

[7] X.Y. Wu, F.A. Dilmanian, Z. Chen, B. Ren, D. N. Slatkin, D. Chapman, M. Shleifer, F. A. Staicu, and W. Thomlinson. Multiple Energy Computed Tomography (MECT) at the NSLS: Status report. Rev. Sci. Instrum. *66*, 1346-1347, 1995.

[8] T. Takeda, Y. Itai, K. Hayashi, Y. Nagata, H. Yamaji, and K. Hyodo, High Spatial Resolution CT with a synchrotron radiation system, J. Comput. Assis. Tomogr. *18*, 98-101, 1994.

[9] J.P. Stonestrom, R.E. Alvarez, and A. Macovski, A framework for spectral artifact corrections in x-ray CT. IEEE Trans. Biom. Eng. *BME-28*, 128-141, 1981.

[10] L. Grodzins, Critical absorption tomography of small samples, Nucl. Instr. and Meth. *206*, 547-552, 1983.

[11] C.E. Cann and H.K. Genant, Precise measurement of vertebral mineral content using computed tomography, J. Comp. Assist. Tomogr. *4*, 493-500, 1980.

[12] E.C. Parsons, et al., Manuscript in preparation.

[13] M. Shleifer, F.A. Dilmanian, F.A. Staicu, and M.H. Woodle, Mechanical design of a high-resolution tunable crystal monochromator for the Multiple Energy Computed Tomography project, Nucl. Instrum. Methods - *A 347*, 356-359, 1994.

[14] Analogic Corp., Peabody, MA 01960.

[15] X.Y. Wu, manuscript in preparation.

[16] J. Kress, "Image Reconstruction and Processing in the MECT Project", M.A. Thesis, Department of Physics, State University of New York at Stony Brook, August 1995.

[17] Gammex RMI, Middleton, WI 53562.

[18] C. Schulze, P. Suortti and D. Chapman, Test of a bent Laue double crystal fixed exit monochromator, Synchr. Radiat. News *3*, 8-11, 1994.